We are IntechOpen, the world's leading publisher of Open Access books
Built by scientists, for scientists

6,900
Open access books available

186,000
International authors and editors

200M
Downloads

154
Countries delivered to

Our authors are among the

TOP 1%
most cited scientists

12.2%
Contributors from top 500 universities

CLARIVATE ANALYTICS
BOOK CITATION INDEX
INDEXED

WEB OF SCIENCE™

Selection of our books indexed in the Book Citation Index
in Web of Science™ Core Collection (BKCI)

Interested in publishing with us?
Contact book.department@intechopen.com

Numbers displayed above are based on latest data collected.
For more information visit www.intechopen.com

Plasmonic Enhancement of Solar Cells Efficiency: Material Dependence in Semiconductor Metallic Surface Nano-Modification

Janusz E. Jacak and Witold A. Jacak

Additional information is available at the end of the chapter

Abstract

Recent experimental data shown a promising direction in employing nano-plasmonics for increasing efficiencies of the solar cells. The effect is due to metallic nanoparticles' plasmons mediating energy transfer from the incoming e-m wave to the semiconductor in a regime violating limits in energy transitions imposed by the momentum conservation, due to translational invariance departure in surface nano-modified system. The chapter presents analysis of material dependence of near-field coupling to band electrons of surface plazmons in metallic nanoparticles deposited on the top of semiconductor substrate in nano-modified solar cells. Various materials for metal and substrate are comparatively studied upon the quantum Fermi Golden Rule approach in theoretical quantitative modeling of the plasmon-electron coupling that enhances ordinary PV effect. The material dependence of the plasmon-mediated efficiency growth in two types of solar cells, multi-crystalline Si and CIGS (copper-indium-gallium-diselenide), modified by various surface-deposited metallic nanoparticles is additionally illustrated by the experimental data.

Keywords: plasmons, metallic nanoparticles, photo effect, solar cells

1. Introduction

The plasmon-mediated sunlight energy harvesting in metal-nano-modified solar cells is caused by three effects: the strong concentration of electric field of plasmon oscillations close to metallic components with local large curvature, the large amplitude of plasmon oscillations in metallic nanoparticles and the enhancement of the probability of interband excitations in semiconductor substrate caused by breaking of the translational symmetry for a nanoparticle

and the dipole near-field coupling of surface plasmons with semiconductor band electrons [1–7]. The transition probability for transfer of electrons from the valence band to the conduction band in a semiconductor, essential for efficiency of the photovoltaic effect, grows due to the electric field amplitude enhancement and due to admission of all oblique transitions not here prohibited by the momentum conservation [4]. In the ordinary photo effect Kiriejew [8], the interband transitions are confined to only vertical ones between states with almost the same momentum due to the momentum conservation and the fact that the sunlight photons have very small momentum (owing to large light velocity, c) which almost does not change electron momentum at scattering: for excitation energy $\hbar\omega$ beyond the forbidden gap, E_g, in the substrate semiconductor, $\hbar\omega = cq$ gives $q \ll p$, where $p \sim \frac{\pi\hbar}{l}$ is the semiconductor band quasi-momentum scale in the Brillouin zone (l denotes here the elementary cell linear size). Thus the change of the band electron momentum $\mathbf{p}_1 = \mathbf{p}_2 + \mathbf{q}$ is negligible on the scale of the Brillouin zone and $\mathbf{p}_1 \simeq \mathbf{p}_2$ (because $c = 10^8$ m/s) and only the vertical, conserving momentum, interband transitions contribute to the ordinary photo effect, i.e., when the transition is caused by free photons with momentum $\mathbf{q}$ and energy $\hbar\omega = cq$.

However, for interaction of band electrons with surface plasmon from the metallic nanoparticle deposited on the semiconductor surface, the situation changes significantly. In the near-field regime [9], the potential of the plasmon dipole on the nanosphere is proportional to $\frac{1}{R^2}$ (R is a distance from the sphere center), which has the infinite decomposition in Fourier picture and thus overlaps with all quasi-momenta in the substrate semiconductor Brillouin zone. This is in contrary to the potential of the free photon which contributes via only single $e^{i(\mathbf{q}\cdot\mathbf{r}-\hbar\omega t)/\hbar}$ plane-wave Fourier component.

The resulted effect of oblique interband transitions can be accounted for via the Fermi Golden Rule (FGR). According the FGR scheme [10], the probability of interband transitions is proportional to matrix element of the perturbation potential between initial and final states and summed up over all initial states in the valence band and over all final states in the conduction band assuming only the energy conservation, $E_p(\mathbf{p}_1) + \hbar\omega = E_n(\mathbf{p}_2)$, where $E_{p(n)}(\mathbf{p})$ is the valence-p (conduction-n) band dispersion and $\hbar\omega$ is the excitation energy related to damped and forced by sunlight surface plasmon oscillations with the bare self-energy value $\hbar\omega_1 = \frac{\hbar\omega_p}{\sqrt{3}}$ (i.e., the Mie energy [11, 12], $\hbar\omega_p = \hbar\sqrt{\frac{n_e e^2}{m^* \varepsilon_0}}$ is the bulk-plasmon energy in metal [13], n_e is the density of collective electrons in metal, m^* is the effective mass of electron in metal, e is the electron charge and ε_0 is the dielectric constant) with not-defined momentum, however. The initial momentum, $\mathbf{p}_1$, and the final one, $\mathbf{p}_2$, can be arbitrary because the momentum conservation is rule out by the matrix element of the local dipole interaction.

The chapter is organized as follows. In Section 2, we present the quantum calculation of the efficiency of photo effect mediated by plasmons in metallic nanoparticles deposited on the top of a semiconductor photodiode. This efficiency has been accounted by application of the Fermi golden rule to the near-field coupling of dipole-plasmons with band electrons in the semiconductor substrate. The resulted transition probability is next utilized to the derivation of the plasmon damping rate due to coupling with band electrons which we present in Section 3.

Section 4 addressed to analysis of the by-plasmon enhanced photo effect efficiency in various materials, including various metals for nanoparticles with plasmons and various semiconductor substrates. Section 5 contains also comparison with experiment both for laboratory Si photodiode covered with metallic nanoparticles as well as for standard solar cells, Si-multicrystal and CIGS.

2. Plasmon-mediated photo effect: Fermi Golden Rule calculus of probability of electron interband excitation due to plasmons

The perturbation of electron band system in the substrate semiconductor due to the presence of dipole surface plasmon oscillations in metallic nanosphere (with a radius a) deposited on the semiconductor surface, has the form of the potential of the e-m field of an oscillating dipole. The Fourier components of the electric $\mathbf{E}_\omega$ and magnetic $\mathbf{B}_\omega$ fields produced in the distance $\mathbf{R}$ from the center of considered nanosphere with the dipole of surface plasmon with the frequency ω, have the form [9],

$$\mathbf{E}_\omega = \frac{1}{\varepsilon}\left\{\mathbf{D}_0\left(\frac{k^2}{R} + \frac{ik}{R^2} - \frac{1}{R^3}\right) + \widehat{\mathbf{n}}(\widehat{\mathbf{n}}\cdot\mathbf{D}_0)\left(-\frac{k^2}{R} - \frac{3ik}{R^2} + \frac{3}{R^3}\right)\right\}e^{ikR} \tag{1}$$

and

$$\mathbf{B}_\omega = \frac{ik}{\sqrt{\varepsilon}}[\mathbf{D}_0 \times \widehat{\mathbf{n}}]\left(\frac{ik}{R} - \frac{1}{R^2}\right)e^{ikR}, \tag{2}$$

(ε is the dielectric permittivity). In the case of the spherical symmetry, the dipole of plasmon is considered as pinned to the center of the nanosphere (the origin of the reference frame system), $\mathbf{D} = \mathbf{D}_0 e^{-i\omega t}$. In Eqs. (1) and (2), we used the notation for the retarded argument, $i\omega\left(t - \frac{R}{c}\right) = i\omega t - ikR$, $\widehat{\mathbf{n}} = \frac{\mathbf{R}}{R}$, $\omega = ck$, momentum $\mathbf{p} = \hbar\mathbf{k}$. The terms with denominators R^3, R^2 and R are referred to near-, medium- and far-field zones of the dipole radiation, correspondingly. Because we consider the interaction with a closely adjacent layer of the substrate semiconductor, all terms with denominators R^2 and R we neglect as small in comparison to the term with R^3 denominator—this is the near-field zone approximation (the magnetic field disappears and the electric field is of the form of a static dipole field [9]). Therefore the related perturbation potential added to the system Hamiltonian attains the form,

$$w = e\psi(\mathbf{R}, t) = \frac{e}{\varepsilon R^2}\widehat{\mathbf{n}}\cdot\mathbf{D}_0\, sin\,(\omega t + \alpha) = w^+ e^{i\omega t} + w^- e^{-i\omega t}. \tag{3}$$

The term $w^+ = (w^-)^* = \frac{e}{\varepsilon R^2}\frac{e^{i\alpha}}{2i}\widehat{\mathbf{n}}\cdot\mathbf{D}_0$ describes emission, i.e., the case of our interest.

According to the FGR [10], the interband transition probability is proportional to

$$w(\mathbf{k}_1, \mathbf{k}_2) = \frac{2\pi}{\hbar}|<\mathbf{k}_1|w^+|\mathbf{k}_2>|^2\delta\big(E_p(\mathbf{k}_1) - E_n(\mathbf{k}_2) + \hbar\omega\big), \tag{4}$$

where the Bloch states in the conduction and valence bands are assumed as planar waves (for simplicity), $\Psi_{\mathbf{k}} = \frac{1}{(2\pi)^{3/2}} e^{i\mathbf{k}\cdot\mathbf{R} - iE_{n(p)}(\mathbf{k})t/\hbar}$, $E_p(\mathbf{k}) = -\frac{\hbar^2\mathbf{k}^2}{2m_p^*} - E_g$, $E_n(\mathbf{k}) = \frac{\hbar^2\mathbf{k}^2}{2m_n^*}$ (indices n, p refer to electrons from the conduction and valence bands, respectively, E_g is the forbidden gap).

The matrix element,

$$< \mathbf{k}_1|w^+|\mathbf{k}_2 > = \frac{1}{(2\pi)^3} \int d^3R \frac{e}{\varepsilon 2i} e^{i\alpha}\hat{\mathbf{n}} \cdot \mathbf{D}_0 \frac{1}{R^2} e^{-i(\mathbf{k}_1-\mathbf{k}_2)\cdot\mathbf{R}}. \tag{5}$$

can be found analytically by a direct integration, which gives the formula ($\mathbf{q} = \mathbf{k}_1 - \mathbf{k}_2$),

$$< \mathbf{k}_1|w^+|\mathbf{k}_2 > = \frac{-1}{(2\pi)^3} \frac{ee^{i\alpha}}{\varepsilon} D_0 \cos\Theta(2\pi) \int_a^\infty dR \frac{1}{q}\frac{d}{dR}\frac{\sin qR}{qR} = \frac{1}{(2\pi)^2}\frac{ee^{i\alpha}}{\varepsilon}\frac{\mathbf{D}_0\cdot\mathbf{q}}{q^2}\frac{\sin qa}{qa}. \tag{6}$$

Next, we must sum up overall initial and final states in both bands. Thus, for the total interband transition probability we have,

$$\delta w = \int d^3k_1 \int d^3k_2 \left[f_1(1-f_2)w(\mathbf{k}_1,\mathbf{k}_2) - f_2(1-f_1)w(\mathbf{k}_2,\mathbf{k}_1) \right], \tag{7}$$

where f_1, f_2 assign the temperature dependent distribution functions (Fermi-Dirac distribution functions) for initial and final states, respectively. For room temperatures, $f_2 \simeq 0$ and $f_1 \simeq 1$, which leads to,

$$\delta w = \int d^3k_1 \int d^3k_2 \cdot w(\mathbf{k}_1,\mathbf{k}_2). \tag{8}$$

After some also analytical integration in the above formula, we arrive at the expression,

$$\delta w = \frac{4}{3}\frac{\mu^2\left(m_n^* + m_p^*\right)2(\hbar\omega - E_g)e^2D_0^2}{\sqrt{m_n^*m_p^*}2\pi\hbar^5\varepsilon^2} \int_0^1 dx \frac{\sin^2(xa\xi)}{(xa\xi)^2}\sqrt{1-x^2}$$

$$= \frac{4}{3}\frac{\mu^2}{\sqrt{m_n^*m_p^*}}\frac{e^2D_0^2}{2\pi\hbar^3\varepsilon^2}\xi^2 \int_0^1 dx \frac{\sin^2(xa\xi)}{(xa\xi)^2}\sqrt{1-x^2}, \tag{9}$$

according to assumed band dispersions, m_n^* and m_p^* denote the effective masses of electrons and holes, $\mu = \frac{m_n^* m_p^*}{m_n^* + m_p^*}$ is the reduced mass, the parameter $\xi = \frac{\sqrt{2(\hbar\omega - E_g)(m_n^* + m_p^*)}}{\hbar}$. In limiting cases for a nanoparticle radius a, we finally obtain,

$$\delta w = \begin{cases} \dfrac{4}{3}\dfrac{\mu\sqrt{m_n^*m_p^*}(\hbar\omega - E_g)e^2D_0^2}{\hbar^5\varepsilon^2}, & \text{for } a\xi \ll 1, \\[3mm] \dfrac{4}{3}\dfrac{\mu^{3/2}\sqrt{2}\sqrt{\hbar\omega - E_g}e^2D_0^2}{a\hbar^4\varepsilon^2}, & \text{for } a\xi \gg 1. \end{cases} \tag{10}$$

In the latter case in Eq. (10), the following approximation was applied,

$$\int_0^1 dx \frac{sin^2(xa\xi)}{(xa\xi)^2}\sqrt{1-x^2} \approx (\text{for } a\xi \gg 1) \frac{1}{a\xi}\int_0^\infty d(xa\xi)\frac{sin^2(xa\xi)}{(xa\xi)^2} = \frac{\pi}{2a\xi},$$

whereas in the former one, $\int_0^1 dx\sqrt{1-x^2} = \pi/4$.

With regard to two limiting cases, $a\xi \ll 1$ or $a\xi \gg 1$, $\xi = \frac{\sqrt{2(\hbar\omega - E_g)(m_n^* + m_p^*)}}{h}$, we see that

$$a \simeq 1/\xi \simeq \begin{cases} > 2\times10^{-9}[m] & \text{for } \frac{\hbar\omega - E_g}{E_g} < 0.02 \\ < 2\times10^{-9}[m] & \text{for } \frac{\hbar\omega - E_g}{E_g} > 0.02 \end{cases}$$, and this range weakly depends on effective

masses and E_g. Thus for nanoparticles with radii $a > 2$ nm, the first regime holds only close to E_g (less than the 2% distance to limiting E_g), whereas the second regime holds in the rest of the

ω domain. For comparison, $a \simeq 1/\xi \simeq \begin{cases} > 0.5\times10^{-9}[m] & \text{for } \frac{\hbar\omega - E_g}{E_g} < 0.5 \\ < 0.5\times10^{-9}[m] & \text{for } \frac{\hbar\omega - E_g}{E_g} > 0.5 \end{cases}$, the first region

widens considerably (to ca. 50% relative distance to E_g), but holds only for ultrasmall size of nanoparticles ($a < 0.5$ nm). For larger nanospheres, e.g., with $a > 10$ nm, the second regime is thus dominating.

One can notice that the above formula, Eq. (9) and its explicit form in limiting situations given by Eq. (10), is the generalization of to the ordinary photo effect, for which the transition probability is different [8],

$$\delta w_0 = \frac{4\sqrt{2}}{3}\frac{\mu^{5/2}e^2}{m_p^{*2}\omega\varepsilon\hbar^3}\left(\frac{\varepsilon E_0^2 V}{8\pi\hbar\omega}\right)(\hbar\omega - E_g)^{3/2}. \tag{11}$$

The number of photons of the ω e-m wave with electric field component amplitude E_0 in the volume V equals to, $\left(\frac{\varepsilon E_0^2 V}{8\pi\hbar\omega}\right)$, hence the probability of single photon absorption by the semiconductor per time unit, attains the form in the ordinary photo effect [8],

$$q_0 = \delta w_0\left(\frac{\varepsilon E_0^2 V}{8\pi\hbar\omega}\right)^{-1} = \frac{4(4)\sqrt{2}}{3}\frac{\mu^{5/2}e^2}{m_p^{*2}\omega\varepsilon\hbar^3}(\hbar\omega - E_g)^{3/2}, \tag{12}$$

(factor (4) corresponds here to spin degeneration of band electrons).

In the case of mediation by plasmons, all oblique interband transitions contribute, not only vertical ones (as it was for the interaction with the planar wave in the ordinary photo effect). This results in an enhancement of the transition probability for the near-field coupling in comparison to the photon (planar wave) absorption rate in a semiconductor in the ordinary photo effect. The enhancement of the probability of transition due to hopping not conserving momentum, is, however, gradually quenched with the radius a growth, as expressed by Eq. (10).

The probability of energy absorption in the semiconductor via mediation of surface plasmons per single photon incident on the metallic nanospheres, q_m, equals to the product of δw (given by Eq. (10)) and the number, N_m, of metallic nanoparticles divided by photon density with additional phenomenological factor β responsible for all effects not directly accounted for (as deposition separation and surface properties reducing the coupling strength, as well as energy losses due to electron scattering and irradiation to far-field zone (Lorentz friction [9]) into upper hemisphere, if the metallic nanoparticle is not completely embedded in the substrate semiconductor medium),

$$q_m = \beta N_m \delta w \left(\frac{\varepsilon E_0^2 V}{8\pi\hbar\omega} \right)^{-1}. \tag{13}$$

3. Damping rate for plasmons in a metallic nanoparticle deposited on a top of a semicoductor

Assuming that the energy acquired by the semiconductor band system, $\mathcal{A}$, is equal to the output of plasmon oscillation energy (resulting in plasmon damping), one can estimate the corresponding damping rate of plasmon oscillations. Namely, at the damped (lowering in time) plasmon amplitude $D_0(t) = D_0 e^{-t/\tau'}$, one finds for a total transmitted energy,

$$\mathcal{A} = \beta \int_0^\infty \delta w \hbar\omega dt = \beta\hbar\omega\delta w \tau'/2 = \begin{cases} \dfrac{2}{3} \dfrac{\beta\omega\tau'\mu\sqrt{m_n^* m_p^*}(\hbar\omega - E_g)e^2 D_0^2}{\hbar^4\varepsilon^2}, & \text{for } a\xi \ll 1, \\[4mm] \dfrac{2}{3} \dfrac{\beta\omega\tau'\mu^{3/2}\sqrt{2}\sqrt{\hbar\omega - E_g}e^2 D_0^2}{a\hbar^3\varepsilon^2}, & \text{for } a\xi \gg 1, \end{cases} \tag{14}$$

where τ' is the damping time-rate and β accounts for losses (not included in the model). Comparing the value of $\mathcal{A}$ given by the formula (14) with the energy loss of damping plasmon estimated in Ref. [4] (the initial energy of the plasmon oscillations which has been transferred step-by-step to the semiconductor, $\mathcal{A} = \frac{D_0^2}{2\varepsilon a^3}$), one can find

$$\frac{1}{\tau'} = \begin{cases} \dfrac{4\beta\omega\mu\sqrt{m_n^* m_p^*}(\hbar\omega - E_g)e^2 a^3}{3\hbar^4\varepsilon}, & \text{for } a\xi \ll 1, \\[4mm] \dfrac{4\beta\omega\mu^{3/2}\sqrt{2}\sqrt{\hbar\omega - E_g}e^2 a^2}{3\hbar^3\varepsilon}, & \text{for } a\xi \gg 1. \end{cases} \tag{15}$$

By τ', we denote here a large damping of plasmons due to energy transfer to the semiconductor substrate highly exceeding the internal damping, characterized by τ, due to scattering of electrons inside the metallic nanoparticle [4] ($\frac{1}{\tau} \ll \frac{1}{\tau'}$). We neglect also the irradiation to far-field upper hemisphere zone of plasmon energy due to the Lorentz friction, which is also smaller than near-field zone energy transfer to the substrate [4].

For example, for nanospheres of Au deposited on the Si layer, we obtain for Mie self-frequency $\omega = \omega_1$,

$$\frac{1}{\tau'\omega_1} = \begin{cases} 44.092\beta\left(\frac{a[nm]}{1[nm]}\right)^3 \frac{\mu}{m} \frac{\sqrt{m_n^* m_p^*}}{m}, & \text{for } a\xi \ll 1, \\ \\ 13.648\beta\left(\frac{a[nm]}{1[nm]}\right)^2 \left(\frac{\mu}{m}\right)^{3/2}, & \text{for } a\xi \gg 1, \end{cases} \tag{16}$$

for light(heavy) carriers in Si, $m_n^* = 0.19(0.98)\ m$, $m_p^* = 0.16(0.52)\ m$, m is the bare electron mass, $\mu = \frac{m_n^* m_p^*}{m_n^* + m_p^*}$ and $E_g = 1.14$ eV, $\hbar\omega_1 = 2.72$ eV. For these parameters and nanospheres with the radius a in the range of $5 - 50$ nm, the lower case of Eq. (16) applies (at $\omega = \omega_1$). The parameter β fitted from the experimental data [4, 14] equals to ca 0.001.

In another scenario when the output of the plasmon energy is recovered by continuous income from the sunlight, one can consider the energy-balanced state. In an idealized case, whole incoming energy of the monochromatic ω e-m wave is transferred to the semiconductor via plasmons, and we deal with the stationary behavior of a driven and damped oscillator for plasmons. Even though the free undamped plasmon has the Mie self-resonance frequency, $\omega_1 = \frac{\omega_p}{\sqrt{3}}$, the frequency of plasma oscillation equals to the driven electric field frequency, ω, of the incident e-m wave of photons. Because of an instant leakage of the plasmon energy in near-field to semiconductor substrate, this large damping of plasmon causes a red-shift and widening of the resonance, as for every damped and driven oscillator. The widened resonance enables the energy transfer from plasmons to electrons to embrace also frequencies lower or larger than Mie frequency but limited from below by the semiconductor gap $E_g/\hbar$.

The incident sunlight dispersion covers the visible spectrum and also some UV and infra-red tails. The total efficiency of the plasmon channel corresponds to a sum (integration) overall Fourier components $\omega > E_g/\hbar$ of light interfered with intensity distribution of sunlight spectrum. To model this behavior, it is necessary to consider separately each single monochromatic e-m mode, i.e., a Fourier component ω. Its electric field excites plasmon with this frequency and this plasmon is damping with the rate $\frac{1}{\tau'}$ (15). This damping causes a red shift of a resonance and reduces the resonance amplitude, which in turn allows for the accommodation to the balance of energy transfer to the semiconductor with incident sunlight e-m wave energy intensity (defined by it electric field amplitude E_0) at the frequency ω. Within this damped and driven oscillator model, the amplitude of plasmon oscillations $D_0(\omega)$ is constant in time and shaped by $f(\omega) = \frac{1}{\sqrt{\left(\omega_1^2 - \omega^2\right)^2 + 4\omega^2/\tau'^2}}$. The extremum of red-shifted resonance is attained at $\omega_m = \omega_1\sqrt{1 - 2(\omega_1\tau')^{-2}}$ with corresponding amplitude $\sim \tau'/\left(2\sqrt{\omega_1^2 - \tau'^{-2}}\right)$. The red shift is proportional to $1/\left(\omega_1\tau'^2\right)$. In the case of the described energy transfer balance, one obtains according to Eq. (10),

$$q_m = \begin{cases} \beta C_0 \dfrac{128}{9}\pi^2 a^3 \dfrac{\mu\sqrt{\mu_n^*\mu_p^*}}{m^2}\left(\hbar\omega - E_g\right)\dfrac{e^6 n_e^2 \omega}{\hbar^4 \varepsilon^3}f^2(\omega), & \text{for } a\xi \ll 1, \\[4mm] \beta C_0 \dfrac{128}{9}\sqrt{2}\pi^2 a^2 \dfrac{\mu^{3/2}}{m^2}\sqrt{\hbar\omega - E_g}\,\dfrac{e^6 n_e^2 \omega}{\hbar^3 \varepsilon^3}f^2(\omega), & \text{for } a\xi \gg 1, \end{cases} \tag{17}$$

where $f(\omega) = \dfrac{1}{\sqrt{\left(\omega_1^2 - \omega^2\right)^2 + 4\omega^2/\tau'^2}}$ corresponds to amplitude factor for driven damped oscillator and $D_0 = \dfrac{e^2 n_e E_0 4\pi a^3}{3m}f(\omega)$ (in Eq. (10)); the amplitude of the electric field, E_0, in the incident e-m wave is next ruled out from Eq. (17) due to normalization per single photon as in Eq. (13); $C_0 = \dfrac{N_m 4/3\pi a^3}{V}$, V is the volume of the semiconductor, N_m is the number of metallic nanospheres.

The ratio, $\dfrac{q_m}{q_0}$, revealing the advantage of the plasmon-mediated photo effect over the ordinary photo effect can be expressed as follows

$$\dfrac{q_m}{q_0} = \begin{cases} \dfrac{4\sqrt{2}\pi^2 a^3 \beta C_0 \sqrt{m_n^* m_p^*}\left(m_p^*\right)^2 e^4 n_e^2 \omega^2 f^2(\omega)}{3\mu^{3/2}m^2\sqrt{\hbar\omega - E_g}\,\hbar\varepsilon^2}, & \text{for } a\xi \ll 1, \\[4mm] \dfrac{8\pi^2 a^2 \beta C_0 \left(m_p^*\right)^2 e^4 n_e^2 \omega^2 f^2(\omega)}{3\mu m^2\left(\hbar\omega - E_g\right)\varepsilon^2}, & \text{for } a\xi \gg 1. \end{cases} \tag{18}$$

This ratio turns out to be of order of $10^4 \dfrac{\beta 40}{H[nm]}$ for the surface density of nanoparticles (as in experiment in Ref. [14]), $n_s \sim 10^8/\text{cm}^2$; note that $C_0 = n_s 4\pi a^3/(3H)$, H is a thickness of the semiconductor layer, which including the phenomenological factor β, and the thickness H (we have confirmed experimentally that the range of the near-field zone exceeds the Mie wavelength), is sufficient to explain the scale of the experimentally observed strong enhancement of absorption rate in semiconductors due to plasmons. The strong enhancement of this transition probability is linked with the allowance of momentum-non-conserved transitions, which is, however, reduced with the radius a growth. The strengthening of the near-field induced interband transitions, in the case of large nanospheres, is, however, still significant as the quenching of oblique interband transitions is partly compensated by $\sim a^3$ growth of the amplitude of dipole plasmon oscillations. The trade-off between these two competing size-dependent factors is responsible for the observed experimental enhancement of light absorption and emission in diode systems mediated by surface plasmons in nanoparticle surface coverings [7, 14–18].

4. Efficiency of the light absorption channel via plasmon for various materials

Nanoparticles of gold and silver (sometimes also of copper) are mostly used in plasmon photovoltaics because their surface plasmon resonances are located within the visible light spectrum. These nanoparticles can be deposited on various semiconductor substrates with different material parameters. We list here the appropriate parameters usable for comparison with experiment

for various configurations of the plasmon solar cell systems. In order to compare with the experiment, we can estimate the photocurrent in the case of a semiconductor photodiode with the metallically modified photoactive surface. This photocurrent is given by $I' = |e|N(q_0 + q_m)A$, where N is the number of incident photons and q_0 and q_m are the probabilities of single photon absorption in the ordinary photo effect [8] and of single photon absorption mediated by the presence of metallic nanospheres, respectively, as derived in the previous paragraph; $A = \frac{\tau_f^n}{t_n} + \frac{\tau_f^p}{t_p}$ is the amplification factor ($\tau_f^{n(p)}$ is the annihilation time of both sign carriers, $t_{n(p)}$ is the drive time for carriers [the time of traversing the distance between electrodes]). From the above formulae, it follows that (here $I = I'(q_m = 0)$, i.e., the photocurrent without metallic modifications),

$$\frac{I'}{I} = 1 + \frac{q_m}{q_0}, \qquad (19)$$

where the ratio q_m/q_0 is given by Eq. (18).

In **Tables 1–3**, we list parameters for several semiconductor substrates and for a metallic nanoparticle few materials, which allow for comparison of the ratio q_m/q_0 for various material configurations by formula (18).

Formula (18) is exemplified in **Figure 1** for Au nanoparticles deposited on Si semiconductor (continuous line)–this reproduces well the experimental behavior (red dashed/dotted) [14]. Both channels of photon absorption resulting in photocurrent in the semiconductor sample are included, the direct ordinary photo effect absorption with probability of transitions given by q_0 and the plasmon-mediated absorption with probability q_m, respectively. Note also that

metal	Bulk pl. (eV)	Surface pl. (eV)
Li	6.6	3.4
Na	5.4	3.3
K	3.8	2.4
Mg	10.7	6.7
Al	15.1	8.8
Fe	10.3	5.0
Cu	6	3.5
Ag	3.8	3.5
Au	4.67	2.7

Table 1. Plasmon energies measured in metals.

metal	Au	Ag	Cu
Mie frequency	4.11×10^{15} 1/s	5.2×10^{15} 1/s	5.7×10^{15} 1/s

Table 2. Mie frequency ω_1 to formula (18).

Semiconductor	m_n^*	m_p^*	E_g
Si	0.9 m L[101], 0.19 m T[110]	0.16 m lh, 0.49 m hh	1.12 eV
GaAs	0.067 m	0.08 m lh, 0.45 m hh	1.35 eV
CIGS	$0.09 - 0.13$ m	0.72 m	$1 - 1.7$ eV

Table 3. Substrate material parameters to formula (18) ($m = 9.1 \times 10^{-31}$ kg, the mass of bare electron; lh–light holes, hh–heavy holes, L–longitudinal, T–transverse).

some additional effects like reflection of the incident photons or destructive interference on metallic net would contribute and it was phenomenologically accounted in the plasmon-mediated channel by an experiment-fitted factor β. The collective interference type corrections are rather not strong for the considered low densities of metallic coverings of order of $10^8/\text{cm}^2$, and nanosphere sizes well lower than the resonant wavelength, though for larger concentrations and larger nanosphere sizes, would play a stronger reducing role (reflecting photons) [6, 19]. The resonance threshold was accounted for the damped resonance envelope function in Eq. (19) including also semiconductor band-gap limit. The relatively high value of $\frac{q_m}{q_0} \sim 10^4 \frac{\beta 40}{H[nm]}$ enables a significant growth of the efficiency of the photoenergy transfer to the semiconductor, mediated by surface plasmons in nanoparticles deposited on the active layer, by increasing β or reducing H (at constant n_s). However, because of the fact that an enhancement of β easily induces the overdamped regime of plasmon oscillations, the more prospective would be lowering of H especially convenient in thin film solar cells. The overall behavior of $I'/I(\omega) = 1 + q_m/q_0$ calculated according to the relation (19), and depicted in **Figure 1**, agrees quite well with the experimental observations [14], in the position, height and shape of the photocurrent curves for distinct samples (the strongest enhancement is achieved for $a = 40$ nm, for Au and Si substrate).

In **Figure 2**, we present the spectral dependence of the plasmonic efficiency enhancement with respect to substrate change (Si, CIGS and GaAs) for the same Au nanoparticles with radius $a = 50$ nm and the same nanoparticle concentration $n_s = 10^8/\text{cm}^2$. One can note that for the CIGS substrate (copper-indium-gallium-diselenide) the spectral characteristics is narrower and
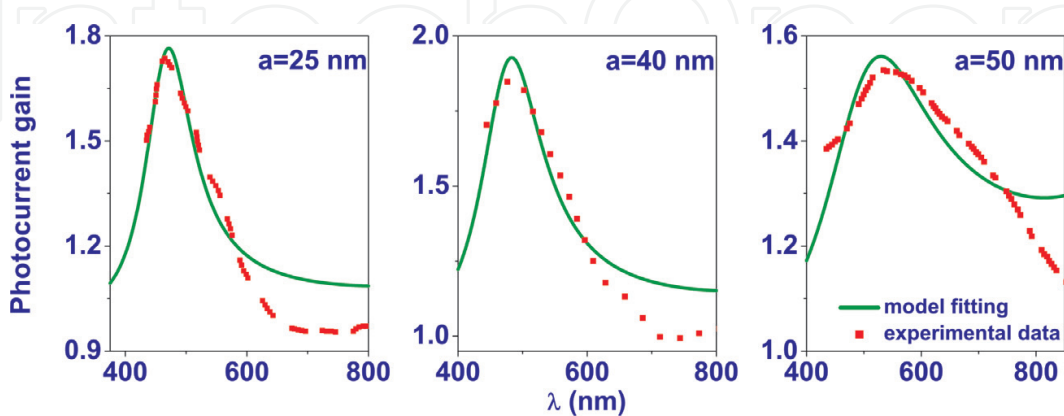

Figure 1. Spectral dependence of the normalized photocurrent $\frac{I'}{I}(\lambda)$ according to formulae (19) and (18)—Comparison with the experimental data (red) from Ref. [14]: $a = 25$ nm, $n_s = 6.6 \times 10^8$ 1/cm^2, (center): $a = 40$ nm, $n_s = 1.6 \times 10^8$ 1/cm^2, (right): $a = 50$ nm, $n_s = 0.8 \times 10^8$ 1/cm^2 ($H = 3$ μm).
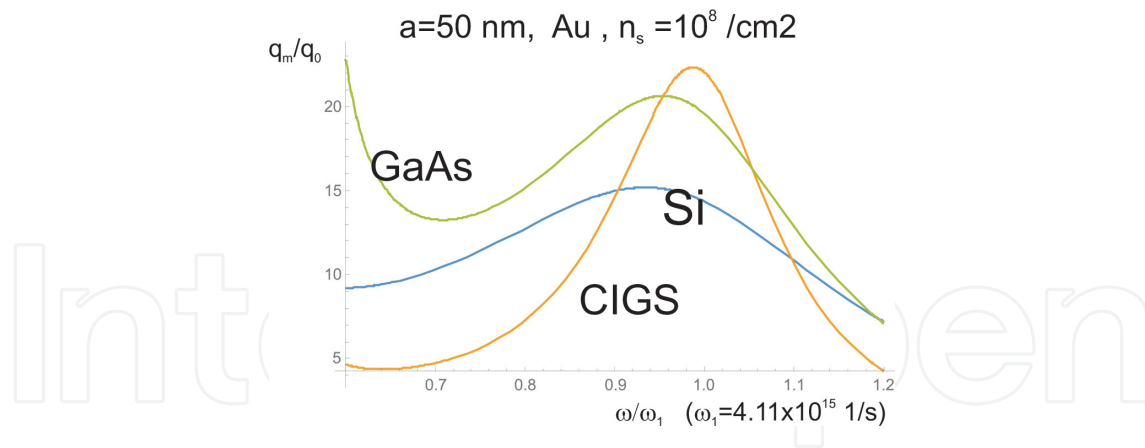
Figure 2. Comparison of the effectiveness of the plasmon channel for Si, GaAs and CIGS substrates with the same Au nanoparticles with radius 50 nm and surface density $10^8/\mathrm{cm}^2$.

blue shifted in comparison to Si and GaAs. **Figure 2** reveals an increase in efficiency of the plasmon effect with growth of the value of forbidden gap E_g conserving other parameters not changed. Especially significantly influential material parameter occurs, however, a mass of holes, cf. **Figure 3**, which is also noticeable from Eq. (18). The mass of holes, $\left(m_p^*\right)^2$, enters the denominator in the formula (12) for the ordinary photo effect and next the numerator in Eq. (18). The higher mass m_p^* the lower efficiency q_0 of the ordinary photo effect is and higher the ratio $\frac{q_m}{q_0}$. In **Figure 4**, the material comparison of metal material of nanoparticles (Au, Ag and Cu) is presented for two their sizes ($a = 50, 25$ nm). The blue shift of spectral characteristics for Ag and Cu in comparison to Au is noticeable (cf. also **Figure 5**) and even more visible for lower radii of nanoparticles due to narrowing of spectral curves (cf. **Figure 6**). From the comparison in **Figures 5** and **6**, for Si and CIGS substrates with Au, Ag and Cu nanoparticles of size $a = 50, 25$ nm (at the nanoparticle concentration $n_s = 10^8/\mathrm{cm}^2$), one can notice that Au nanoparticles utilize the visible spectrum in the better manner than Ag or Cu ones. The advantage of Au nanoparticles is greater in the case of Si substrate and is reduced for CIGS
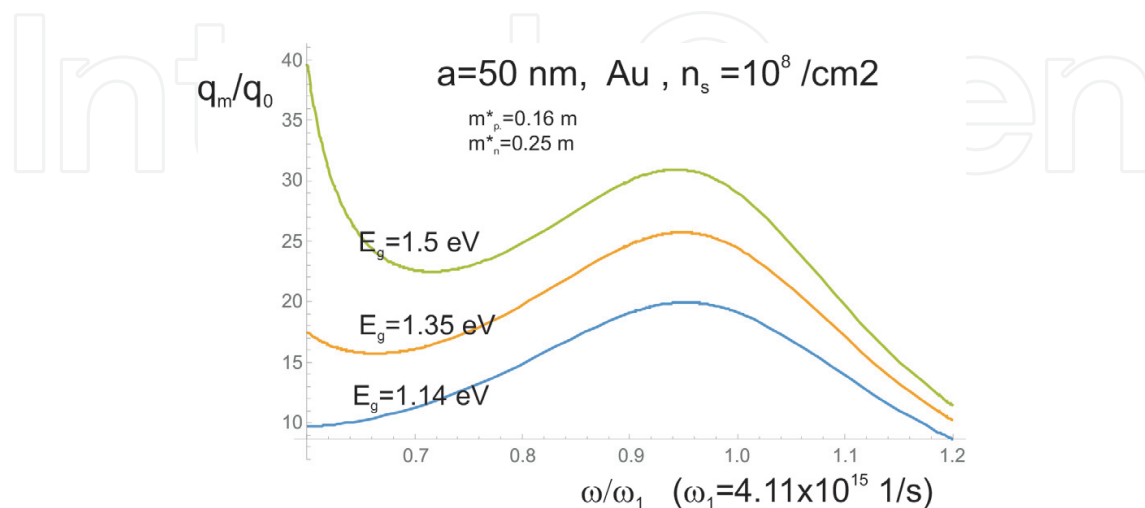

Figure 3. Comparison of the effectiveness of the plasmon channel for varying E_g but the same effective masses of substrates covered with the same Au nanoparticles with radius 50 nm and surface density $10^8/\mathrm{cm}^2$.
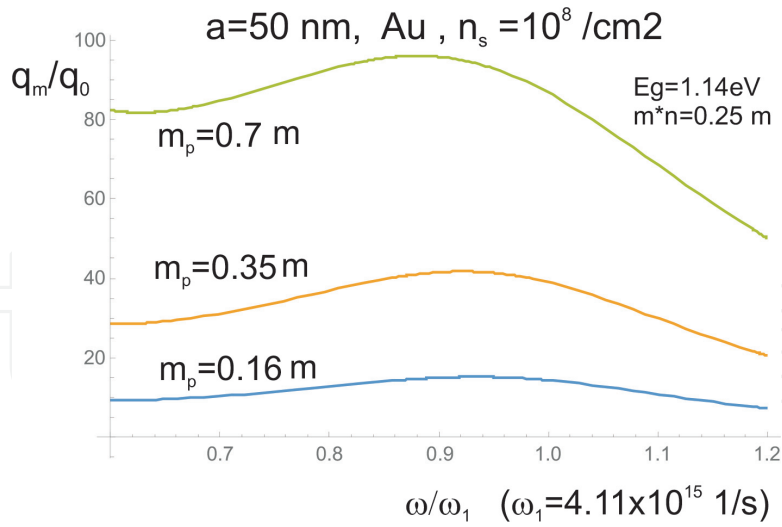
Figure 4. Comparison of the effectiveness of the plasmon channel for varying hole mass m_p^* but the same electron mass and E_g of substrates covered with the same Au nanoparticles with radius 50 nm and surface density $10^8/cm^2$.
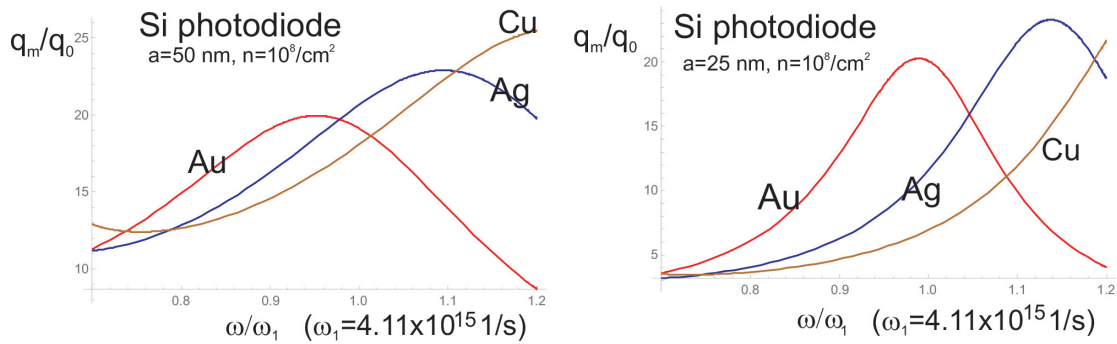

Figure 5. Comparison of the effectiveness of the plasmon channel for the same substrate Si with Au (red), Ag (blue) and Cu (brown) nanoparticles of the same radius 50 nm and surface density $10^8/cm^2$.

substrate because the blue shift of E_g in CIGS with respect to Si. In the case of CIGS (especially for large nanoparticles, $a = 50$ nm), the advantage of Au beyond Ag in overall utilization of sunlight spectrum disappears, whereas is pronounced in the case of Si substrate. Later, we describe an experimental confirmation of this behavior of Si and CIGS substrates, at laboratory sunlight-type illumination by Yamashita DensoYSS-50Aunder AM1.5 [19].

For nanoparticles of gold (Au) and silver (Ag) of size, $a = 50$ nm, optimized due to formula (18), deposited on the multi-crystalline silicon (mc-Si) and on the copper-indium-gallium-diselenide (CIGS) solar cells, the measured [19] overall increase of cell efficiency attains the level of even 5%. The application of suitable concentration of Au and Ag nanoparticles onto mc-Si solar cells increases their efficiency by 5.6 and 4.8%, respectively [19]. Application of Au and Ag nanoparticles onto surface of CIGS solar cells improves their efficiency by 1.2 and 1.4%, respectively [19]. This is visualized in **Figures 7** and **8**, where it is compared an increase in solar cell overall efficiency (the ratio of the field beneath the I-V curve for the metallically improved solar cell and the clean solar cell; the same size (50 nm for radius) and the same
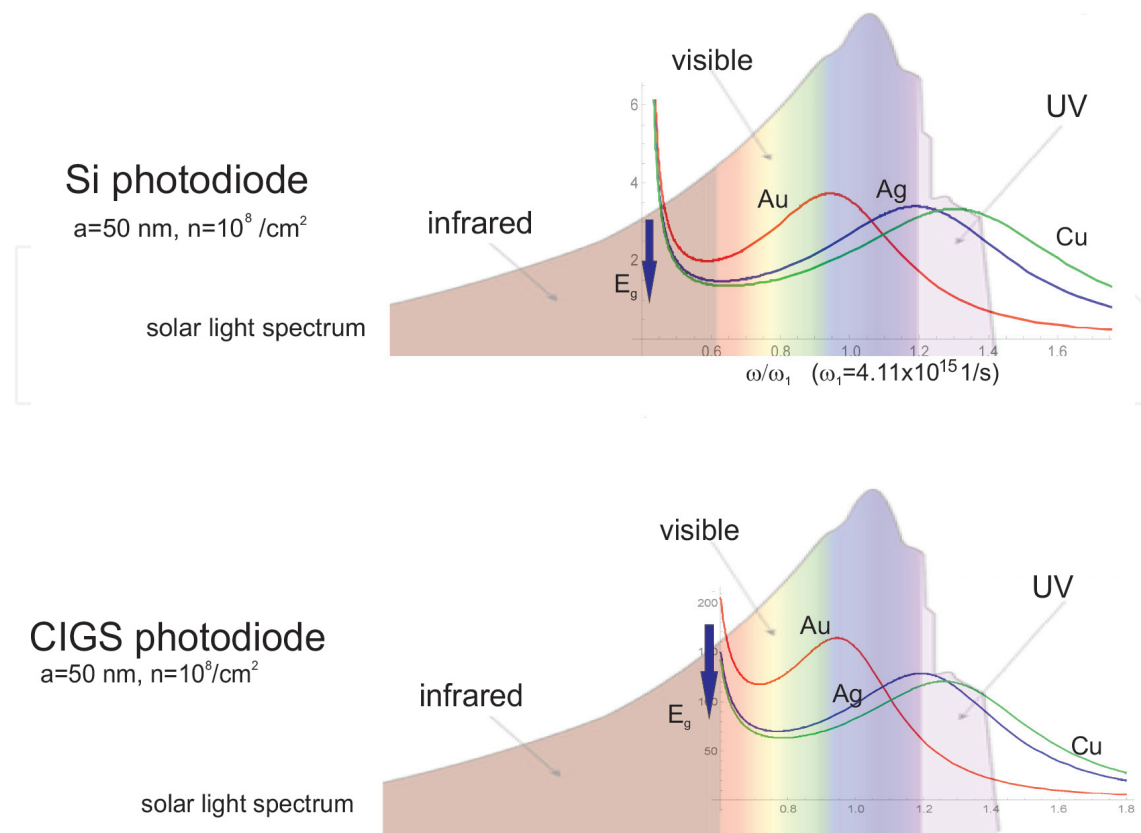
Figure 6. Comparison of the effectiveness of the plasmon channel for the same substrate Si (upper) and CIGS (lower) with Au (red), Ag (blue) and Cu (green) nanoparticles of the same radius 50 nm and surface density $10^8/\text{cm}^2$, versus the sunlight spectrum on the earth surface.

concentration (from the 5% colloidal solution sputtering over the surface) has been applied to different samples)—for more detail cf. Ref. [19].

Worth noting is an agreement of experimentally observed difference in the increase of the efficiency due to the plasmon effect in both cases, of mc-Si and CIGS cells, if one compares the results of application of Au and Ag particles (at the same size of metallic nanoparticles and the same their surface concentration). This behavior agrees with the theoretical study of the material dependence of the plasmon effect, as shown above. From **Figures 2–5**, we see that for Si substrate Au nanoparticles with radii 50 nm better utilize the solar light spectrum than Ag or Cu particles (cf. **Figure 5**), and indeed in the experiment (cf. **Figure 8**) for Au nanoparticles the efficiency growth is ca. 10% larger than for Ag nanoparticles of the same size and concentration on the substrate m-Si solar cell. Interestingly, for the substrate CIGS cell, the effect is weaker and inverted, cf. **Figure 9**. This also is noticeable from the theoretical modeling—due to different E_g and effective masses of carriers for CIGS with respect to mc-Si. The maxima for efficiency enhancement for Au and Ag mutually shift in such a way that for CIGS Ag nanoparticles a bit better suit to solar light spectrum than Au nanoparticles. However, to analyze these effects in more detail, a measurement of spectral characteristics of all considered structures at varying but monochromatic illumination uniformly calibrated should be performed.
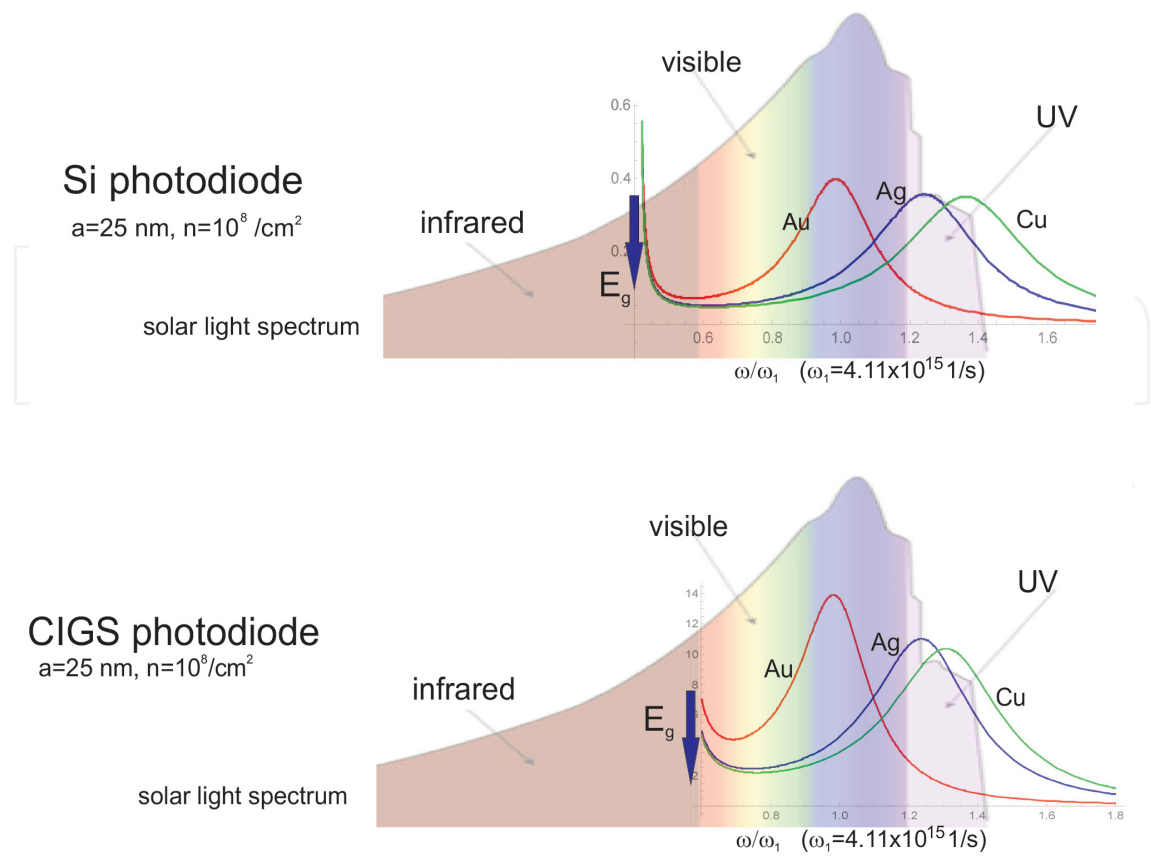
Figure 7. Comparison of the effectiveness of the plasmon channel for the same substrate Si (upper) and CIGS (lower) with Au (red), Ag (blue) and Cu (green) nanoparticles of the same radius 25 nm and surface density $10^8/cm^2$, versus the sunlight spectrum on the earth surface.
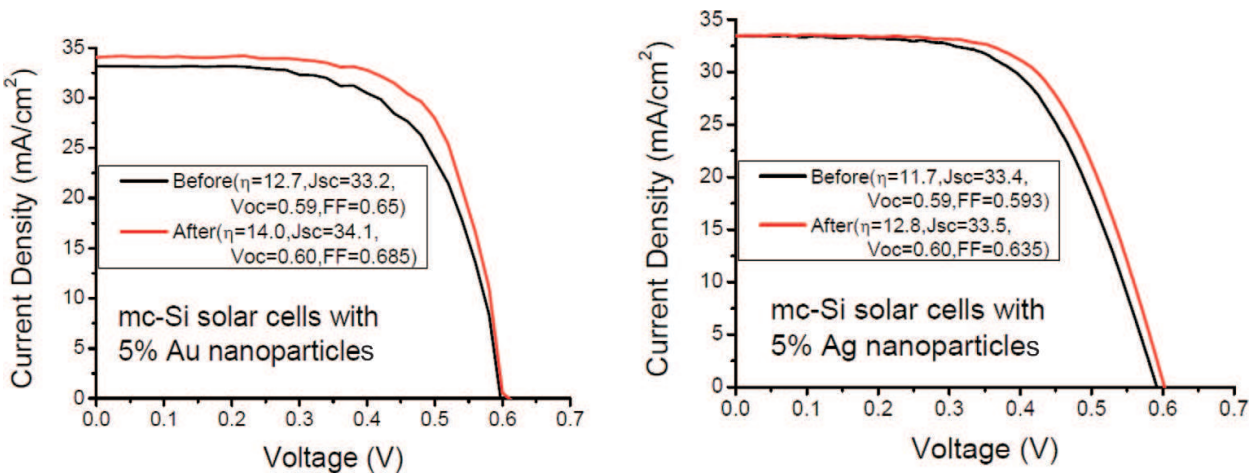

Figure 8. Comparison of solar cell efficiency due to plasmon modification for the multi-crystal Si solar cell, (left) modified by Au nanoparticles, (right) by Ag nanoparticles [19].
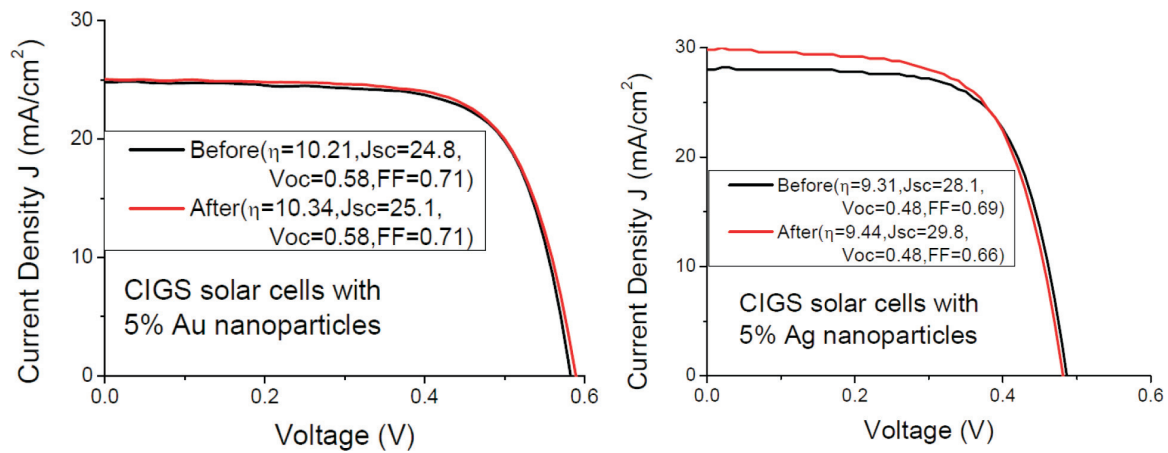
Figure 9. Comparison of solar cell efficiency due to plasmon modification for the CIGS cell, (left) modified by Au nanoparticles, (right) by Ag nanoparticles [19].

5. Conclusion

We have demonstrated by application of the Fermi Golden Rule scheme, that the efficiency of the energy transfer channel between the surface plasmon oscillations in a metallic nanoparticles and a substrate semiconductor depends on parameters of both deposited metallic particles (its radius and material) as well as on semiconductor parameters (energy gap, and effective masses of electron and holes). Found by us formula which generalizes the ordinary photo effect onto the plasmon-mediated one, agrees well with the experimental measurements in laboratory photodiode configuration. The measured ratio of photocurrent in the setup with and without metallic nano-components is compared with the theoretically predicted scenario. The quantitative consistence is obtained both in the shape of the spectral characteristics and in the particle size dependence (as illustrated for Si diode with deposited Au nanoparticles with radii 25, 40 and 50 nm). The qualitative agreement has been achieved also for complete solar cells where the plasmon effect is obscured by other elements of the long series of effects resulting in overall solar cell efficiency beyond only efficiency of the absorption of photons. We have compared the experimental data for multi-crystalline Si solar cell and CIGS (copper-indium-gallium-diselenide) solar cell covered or not with gold and silver nanoparticles with radii of order of 50 nm. The increase of the overall photovoltaic efficiency for metallically modified cells varies between 1.5 (CIGS) and 6% (Si), depending on nanoparticle concentration (for too dense concentration the efficiency drops down). A bit better increase (ca. 10% difference) causes Au nanoparticles for Si cell in comparison to Ag nanoparticles, whereas for CIGS cell, the difference between effect of Ag nanoparticles and Au ones is inverted and strongly reduced. This also agrees qualitatively with theory predictions taken into account differences in Mie frequency in Au and Ag and also different semiconductor parameters for Si and CIGS.

Author details

Janusz E. Jacak and Witold A. Jacak*

*Address all correspondence to: witold.aleksander.jacak@pwr.wroc.pl

Department of Quantum Technology, Wrocław University of Science and Technology, Poland

References

[1] Atwater HA, Polman A. Plasmonics for improved photovoltaic devices. Nature Materials. 2010;**9**:205

[2] Catchpole KR, Mokkapati S, Beck F, Wang E, McKinley A, Basch A, Lee J. Plasmonics and nanophotonics for photovoltaics. MRS Bulletin. 2011;**36**:461-467

[3] Green MA, Pillai S. Harnessing plasmonics for solar cells. Nature Photonics. 2012;**6**:130-132

[4] Jacak J, Krasnyj J, Jacak W, Gonczarek R, Chepok A, Jacak L. Surface and volume plasmons in metallic nanospheres in semiclassical RPA-type approach; near-field coupling of surface plasmons with semiconductor substrate. Physical Review B. 2010;**82**:035418

[5] Lee J, Peumans P. The origin of enhanced optical absorption in solar cells with metal nanoparticles embedded in the active layer. Optics Express. 2010;**18**:10078

[6] Losurdo M, Giangregorio MM, Bianco GV, Sacchetti A, Capezzuto P, Bruno G. Enhanced absorption in Au nanoparticles/a-Si:H/c-Si heterojunction solar cells exploiting au surface plasmon resonance. Solar Energy Materials & Solar Cells. 2009;**93**:1749

[7] Pillai S, Catchpole KR, Trupke T, Zhang G, Zhao J, Green MA. Enhanced emission from Si-based light-emitting diodes using surface plasmons. Applied Physics Letters. 2006;**88**(161102)

[8] Kiriejew PS. Physics of Semiconductors. Warsaw: PWN; 1969

[9] Landau LD, Lifshitz EM. Field Theory. Moscow: Nauka; 1973

[10] Landau LD, Lifshitz LM. Quantum Mechanics. Nonrelativistic Theory. Pergamon Press; 1965

[11] Bohren CF, Huffman DR. Absorption and Scattering of Light by Small Particles. New York: Wiley; 1983

[12] Mie G. Beitrige zur Optik trüber Medien, speziell kolloidaler Metallösungen. Annals of Physics. 1908;**25**:376

[13] Pines D. Elementary Excitations in Solids. Massachusetts: ABP Perseus Books; 1999

[14] Schaadt DM, Feng B, Yu ET. Enhanced semiconductor optical absorption via surface plasmon excitation in metal nanoparticles. Applied Physics Letters. 2005;**86**:063106

[15] Okamoto K, Niki I, Shvartser A, Narukawa Y, Mukai T, Scherer A. Surface plasmon enhanced spontaneous emission rate of InGaN/GaN QW probed by time-resolved photolumimnescence spectroscopy. Nature Materials. 2004;**3**:601

[16] Stuart HR, Hall DG. Enhanced dipole-dipole interaction between elementary radiators near a surface. Physical Review Letters. 1998:80

[17] Wen C, Ishikawa K, Kishima M, Yamada K. Effects of silver particles on the photovoltaic properties of dye-sensitized TiO_2 thin films, *Sol*. Cell. 2000;**61**:339

[18] Westphalen M, Kreibig U, Rostalski J, Lüth H, Meissner D. Metal cluster enhanced organic solar cells. Solar Energy Materials & Solar Cells. 2000;**61**:97

[19] Jeng M, Chen Z, Xiao Y, Chang L, Ao J, Sun Y, Popko E, Jacak W, Chow L. Improving efficiency of multicrystalline silicon and CIGS solar cells by incorporating metal nanoparticles. Materials. 2015;**8**:6761